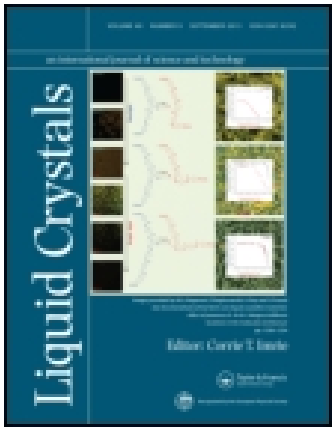

Liquid Crystals

Publication details, including instructions for authors and subscription information:
http://www.tandfonline.com/loi/tlct20

Dynamics of peristrophic multiplexing in holographic polymer-dispersed liquid crystal

Zhenghong He[ab], Chao Ping Chen[a], Hongyue Gao[a], Qiang Shi[a], Shui Liu[c], Xiao Li[a], Yuan Xiong[a], Jiangang Lu[a], Gufeng He[a] & Yikai Su[a]

[a] National Engineering Laboratory of TFT-LCD Materials and Technologies, Department of Electronic Engineering, Shanghai Jiao Tong University, Shanghai, China

[b] School of Physical Science and Technology, Southwest University, Chongqing, China

[c] School of Electronic and Optical Engineering, Nanjing University of Science and Technology, Nanjing, Jiangsu, China

Published online: 13 Jan 2014.

To cite this article: Zhenghong He, Chao Ping Chen, Hongyue Gao, Qiang Shi, Shui Liu, Xiao Li, Yuan Xiong, Jiangang Lu, Gufeng He & Yikai Su (2014) Dynamics of peristrophic multiplexing in holographic polymer-dispersed liquid crystal, Liquid Crystals, 41:5, 673-684, DOI: 10.1080/02678292.2013.875226

To link to this article: http://dx.doi.org/10.1080/02678292.2013.875226

Liquid Crystals, 2014
Vol. 41, No. 5, 673–684, http://dx.doi.org/10.1080/02678292.2013.875226

Taylor & Francis
Taylor & Francis Group

Dynamics of peristrophic multiplexing in holographic polymer-dispersed liquid crystal

Zhenghong He[a,b], Chao Ping Chen[a]*, Hongyue Gao[a], Qiang Shi[a], Shui Liu[c], Xiao Li[a], Yuan Xiong[a], Jiangang Lu[a], Gufeng He[a] and Yikai Su[a]*

[a]*National Engineering Laboratory of TFT-LCD Materials and Technologies, Department of Electronic Engineering, Shanghai Jiao Tong University, Shanghai, China;* [b]*School of Physical Science and Technology, Southwest University, Chongqing, China;* [c]*School of Electronic and Optical Engineering, Nanjing University of Science and Technology, Nanjing, Jiangsu, China*

(*Received 26 July 2013; accepted 10 December 2013*)

In this article, we derive a two-dimensional nonlocal diffusion model utilising finite difference time domain method, which describes the dynamics of how multiple holographic gratings are formed in a polymer-dispersed liquid crystal film for peristrophic multiplexing storage. This model takes into account the diffusion processes of both the free monomer and the liquid crystal molecules, and the polymerisation kinetics in the overlapped regions of multiple holographic gratings. We have experimentally found out that there exists a bounce in the diffraction efficiency for multiplexed gratings at relatively low-exposure intensities, which is undesirable for recording the equal-strength holograms. Instead, the equal-strength holograms can be stored under relatively high-exposure intensities. To predict the occurrence of bounce, the temporal evolutions of the refractive index modulation are estimated and then verified by the experimental results. The appropriate holographic exposure intensity for recording the equal-strength hologram is suggested.

Keywords: holographic gratings; peristrophic multiplexing; PDLC; diffraction efficiency; diffusion equations

1. Introduction

Polymer-dispersed liquid crystal (PDLC) has received considerable interests as a holographic recording material over two decades. This material can be used to fabricate volume Bragg gratings, Fresnel lenses, high-resolution optical storage, etc., due to its unique and attractive optical properties.[1–8] There have been extensive studies on holographic polymer-dispersed liquid crystal (HPDLC) and demonstrations of some functional prototypes. The characteristics of one dimensional (1D) holographic grating formation have been examined in several studies. Rhee et al. experimentally studied the temporal properties of holographic formation in DuPont photopolymers.[9] Zhao and Mouroulis proposed a 1D reaction-diffusion model to describe the process of holographic photopolymerisation in photocurable monomer molecules.[10] Liu et al. developed an analytical method based on conventional reaction-diffusion model.[8] A number of 1D models describing the formation dynamics of the volume Bragg gratings have either been proposed or revised.[11–17] However, most of these established models are limited to 1D holographic grating and optically isotropic media.

Kloosterboer et al. proposed the thermodynamic models for phase separation induced by the increase of network elasticity and polymerisation on the formation of PDLCs, and measured by simultaneous photo DSC/turbidity.[18–20] Sutherland et al. developed a 1D phenomenological model of hologram formation, and incorporated the photophysics and photochemistry, but they were not applicable to describe the dynamics and performance of multiplexed HPDLC gratings, and the nonlocal response of polymer chains were ignored.[21–23] Kyu et al. explored LC phase separation and two-dimensional (2D) photonic structures in an LC-polymer mixture through numerically solving the coupled time-dependent Ginzburg-Landau equations with sinusoidal photopolymerisation.[24–28] Their studies are useful for modelling the development of PDLC and HPDLC, but both of them are incapable of modelling the real-time diffraction properties.

During the peristrophic multiplexing storage, a following grating is formed on the previous one. The spatial diffusion caused by the gradient of the free monomer concentration can affect the refractive index of the existing holographic gratings during the multiplexing processes. Furthermore, the multiplexing processes make the formation kinetics of the multiple holographic gratings more complicated than that of single holographic grating. In order to describe the diffusion behaviours for multiplexed 2D gratings, i.e., the diffusions along both x and y directions, it is necessary to extend the 1D model to a 2D diffusion model.

*Corresponding authors. Emails: ccp@sjtu.edu.cn (C.P. Chen), yikaisu@sjtu.edu.cn (Y. Su)

In this article, a 2D nonlocal diffusion model utilising finite difference time domain (FDTD) technique is proposed. The dynamic behaviours of the formation of multiple holographic gratings in PDLC cell are numerically simulated and experimentally studied using real-time diffraction-monitoring technique under the relatively high- and relatively low-exposure intensities, respectively. In this study, it is found out that our model is able to predict and explain the occurrence of a bounce in diffraction efficiency under the low-intensity exposure condition. In the presence of bounce, the obtained results suggest that it is impossible to balance diffraction efficiencies for all multiplexed gratings. Based on the proposed model, the equal diffraction efficiencies of the multiple gratings can be realised by the optimised time under the high-intensity exposure conditions. The proposed 2D nonlocal diffusion model utilising FDTD technique is useful to extract estimates of key material parameters from experimentally obtained results. This work is particularly important for high-capacity holographic storage with equal-strength holograms.

2. Theory: 2D nonlocal diffusion model

PDLC is made from a homogenous mixture of prepolymer and LC. As the free monomers in the prepolymer are polymerised, the LC molecules separate as a distinct micro-droplet phase.[29,30] The polymerised monomers are 'locked in' a periodic structure of alternating LC-rich and polymer-rich layers. The LC rich regions contain randomly oriented micro-droplets. The symmetry axes of the LC droplets orientate randomly, and the refractive index mismatches between the LC droplets and the polymer chains. As a result, it creates a refractive index difference and coherent scattering condition.[29] According to the 1D reaction-diffusion model proposed by Zhao and Mouroulis,[10] when a layer of PDLC mixture is exposed to a holographic optical field, polymer networks are primarily formed in locations under the bright regions, attracting monomer molecules to diffuse from the dark regions due to concentration gradient. In the meantime, the LC molecules diffuse with a greater diffusivity due to the significantly lower molecular weight than the free monomer molecules, thus aggregating in the dark regions to preserve volume conservation.[29–31] This process results in a refractive index modulation (RIM) in the exposed region of the PDLC cell, forming a volume Bragg grating which diffracts the light that passes through. It was shown that the HPDLC acted as an isotropic volume grating once the free monomer concentration was higher than 24%, where the conventional Kogelnik's diffraction theory for isotropic holographic gratings could be applied.[32–34]

For a holographic exposure where two coherent light beams intersect at a certain angle, alternative bright and dark interference fringes of the transverse light are formed. The light intensity can be expressed by $I(x) = I_0\,[1 + V\cos(\vec{K}\cdot x)]$ where $I_0 = I_1 + I_2$ is the sum of the intensities of the two interfering beams, I_1 and I_2, and V is a constant of the visibility of the fringes. $\vec{K}$ is the grating vector with amplitude $K = 2\pi/\Lambda$, and Λ is the grating period. For the material system, TMPTA is a multi-functional acrylate monomer, whose reaction behaviours are different than the mono-functional monomers. However, liquid–liquid phase separation accompanied with diffusion still holds for the multi-functional acrylate monomer when mixed with LC during the holographic exposure.[24,26] Moreover, the reaction-diffusion in the multi-dimensional multiplexed gratings is way more complex than that in single exposure. For the sake of simplifying our model, we resort to the classical reaction-diffusion equation.[10–12,15–17]

We then propose the use of Equation (1) to govern the 2D polymerisation process based on the 1D reaction-diffusion model.[10,12,13] Then, the 2D nonlocal diffusion equation describing the free monomer diffusion as well as depletion during the exposure can be written as [12]

$$\begin{aligned}\frac{\partial \Phi_{\mathrm{M}}(x,y,t)}{\partial t} &= \frac{\partial}{\partial \mathrm{x}}\left[D(x,y,t)\frac{\partial \Phi_{\mathrm{M}}(x,y,t)}{\partial x}\right] \\ &\quad + \frac{\partial}{\partial \mathrm{y}}\left[D(x,y,t)\frac{\partial \Phi_{\mathrm{M}}(x,y,t)}{\partial y}\right] \\ &\quad - \int_{-\infty}^{\infty}\!\!\int G(x,x';y,y')\cdot F(x',y')\cdot \Phi_{\mathrm{M}}(x,y,t)\,dx'\,dy',\end{aligned} \tag{1}$$

where $\Phi_{\mathrm{M}}(x,y,t)$ is the free monomer concentration, $D(x,y,t)$ is the diffusion coefficients, $F(x',y')$ is the polymerisation rate constant, and $G(x,x';y,y')$ is the nonlocal response function representing the effect of the free monomer concentration at the location (x',y') on the amount of monomer polymerised at location (x,y).[11,12] The key feature of the nonlocal model is to take into account the formation of growing polymer chains, which extend in space rather than reside at a local point, and they would affect the quality of the interference pattern during the growth.

The relation between the polymerisation rate constant $F(x,\ y)$ and the exposure intensity $I(x,\ y)$ is expressed in Equation (2), and the relation between the diffusion coefficient $D(x,y,t)$ and the concentration

of the polymerised monomer, i.e., $\Phi_P(x,y,t)$ are expressed in Equation (3), respectively.

$$F(x,y) = \kappa I_0^v \left[1 + V\cos(\vec{K}\cdot\vec{r})\right]^v, \tag{2}$$

$$D(x,y,t) = D_0 \exp[-\alpha \Phi_P(x,y,t)], \tag{3}$$

where κ is a proportionality coefficient, v is the exponent of the relationship between the polymerisation rate constant and exposure intensity I_0, and in the range 0.82–0.94 in the most of the multifunctional monomer systems,[27] α is the decay parameter of the diffusion coefficient, D_0 represents the initial diffusion constant, and $\vec{r}$ is the direction vector.

For a given exposure time t, the concentration of polymer, $\Phi_P(x,y,t)$ at the location $(x,\ y)$ is given by Equation (4) [10,11]

$$\Phi_P(x,y,t) = \int_0^t \int_{-\infty}^{\infty} G(x,x';y,y') \cdot F(x',y') \Phi_M(x',y',t') dx' dy' t', \tag{4}$$

Furthermore, a Gaussian probability distribution function $G(x,x';y,y')$ to describe the non-local material spatial response can be expressed as [13–17]

$$G(x,x';y,y') = \frac{1}{2\pi\sigma} \exp\left[\frac{-(x-x')^2-(y-y')^2}{2\sigma}\right], \tag{5}$$

where $\sqrt{\sigma}$ represents the nonlocal-response length normalised with respect to the grating period, Λ.[13–17] $G(x,x';y,y')$ represents the effect of chain initiation at location (x,y) on the amount of the polymer at location (x',y').[13–17] $\sqrt{\sigma}$ is an important parameter when considering the data storage capacity or recording resolution within a photopolymer material.

The holographic recording material applied in this work is a TMPTA-based PDLC. If the polymerisation of monomers is subject to a holographic exposure consisting of alternating bright and dark interference fringes, there will exist different monomer concentration gradients across these regions, which would in turn drive monomer molecules to diffuse from the low-depleted regions to highly depleted regions. However, the free radical molecules are at the much excited states (after the electron transfer), and they tend to interact with free monomers to mediate polymerisation. Since the above processes take place for a very short period of time, it is unlikely for those radicals to diffuse even at a tiny distance. Moreover, the molecular weight of radicals is usually heavier than that of free monomers, hence less mobility. [15,16,25,26] For the above reasons, we treat the diffusion of monomer with reaction-diffusion equations and that of radicals as negligible.

The volume shrinkage or contraction is also treated to be negligible, therefore the mass conservation holds in the sample cell throughout the process of holographic exposure. Applying the Lorentz-Lorenz relation,[15–17,35–37] the variation of the refractive index of the PDLC can be estimated. In order to do so, the volume fractions and refractive indices of the individual components of PDLC must be specified. The volume fraction of each component can be expressed as $\phi_i = x_i v_i / \sum_i x_i v_i$, where x_i is the mole fraction and v_i is the molar volume of the i^{th} component. In this case, we assume that the total volume fraction is conserved, then

$$\Phi_M(x,y,t) + \phi_P(x,y,t) + \phi_{LC}(x,y,t) = 1, \tag{6}$$

where $\phi_M(x,y,t)$, $\phi_P(x,y,t)$, $\phi_{LC}(x,y,t)$ denote the volume fractions for the free monomer, polymer, and LC, respectively. The average refractive index (ARI), n, of a given material layer of PDLC can be written as [37]

$$\frac{n^2-1}{n^2+2} = \phi_M \frac{n_M^2-1}{n_M^2+2} + \phi_P \frac{n_P^2-1}{n_P^2+2} + \phi_{LC} \frac{n_{LC}^2-1}{n_{LC}^2+2}, \tag{7}$$

where $n_M = 1.487$ and $n_P = 1.522$ refer to the refractive indices of the free monomer and polymer, respectively, and $n_{LC} \approx \sqrt{(2n_o^2 + n_e^2)/3} = 1.592$ ($n_e = 1.706$, $n_o = 1.532$, at $\lambda = 632.8$ nm) is the ARI of LC.[3,8,38] RIM for each grating can be thus defined as

$$\Delta\bar{n} = \left|\bar{n}_{\text{Bright}} - \bar{n}_{\text{Dark}}\right|, \tag{8}$$

where $\bar{n}_{\text{Bright}}$ and $\bar{n}_{\text{Dark}}$ are the average refractive indices of the bright and dark regions formed under the holographic exposure, respectively. The average diffraction efficiency of the first holographic grating can be expressed [2,32,39,40] as

$$\bar{\eta} = \sin^2\left(\frac{\pi d(1-r)\Delta\bar{n}}{\lambda\cos\theta}\right), \tag{9}$$

where d is the thickness of PDLC film, θ is the Bragg angle, and $\Delta\bar{n}$ is the RIM in Equation (8). r is the erasing

coefficient in the process of peristropic multiplexing, and $r = 0$ for the single holographic grating.[2]

3. Dynamics of peristrophic multiplex based on two holographic gratings

To illustrate the dynamics of 2D holographic grating formation for peristrophic multiplexed storage, Equations (1)–(5) are solved using FDTD method with initial experimental conditions of the free monomer concentration $\Phi_M = 1.79$ mmol cm^{-3}, the LC concentration $\Phi_{LC} = 1.942$ mmol cm^{-3}, grating period $\Lambda = 1.03$ μm, respectively. The parameters are assigned to be $V = 0.95$, $v = 0.9$, $\alpha = 2.7$,[28] and the time increment $\Delta t = 0.01$ s.

The evolutions of the volume fraction of each component and the diffraction efficiencies for the multiple gratings can be predicted by substituting the obtained spatial concentrations $\Phi_M(x,y,t)$, $\Phi_P(x,y,t)$, and $\Phi_{LC}(x,y,t)$ into Equations (6–9). Two holographic gratings are recorded at one single location using the peristrophic multiplexing technique. In details, the first grating stored with the grating vector of 0° is called 0° grating. After 0° grating is completed, the second grating is stored upon the 0° grating with 45° rotation about the normal of sample surface, which is therefore called 45° grating. The schematic multiplexed gratings and overlapped regions of the 0° and 45° are shown in Figure 1, where each region is denoted by a Roman number. In order to examine the diffusion dynamics under the different intensities I_0, a low intensity (2.5 mW cm^{-2}) and a high intensity (19.6 mW cm^{-2}) are applied for comparison. The entire process of each exposure consists of two stages for peristrophic multiplexing storage, one is holographic exposure and the other is postcuring while the exposing light is turned off. The total exposure times t_{sum} for 2.5 and 19.6 mW cm^{-2} are 40.0 and 16.0 s, respectively. The exposure times are denoted as t_1, and t_2, for the first and the second exposure under each exposure intensity, respectively. The postcuring time is therefore $t_{sum} - t_i$, where $i = 1$ and 2. When $I_0 = 2.5$ mW cm^{-2}, the exposure time is $t_1 = t_2 = 20.0$ s, and when $I_0 = 19.6$ mW cm^{-2}, $t_1 = t_2 = 2.55$ s. It is necessary to note that the exposure times are adjusted to ensure equal dosage to be delivered to the material sample.

3.1 *Diffusion dynamics under the low intensity*

Figure 2 depicts the time evolution of the volume fraction of each material component within the overlapped regions of 0° and 45° gratings during the second exposure under $I_0 = 2.5$ mW cm^{-2}. The overlapped regions are referred as I, II, III, and IV as

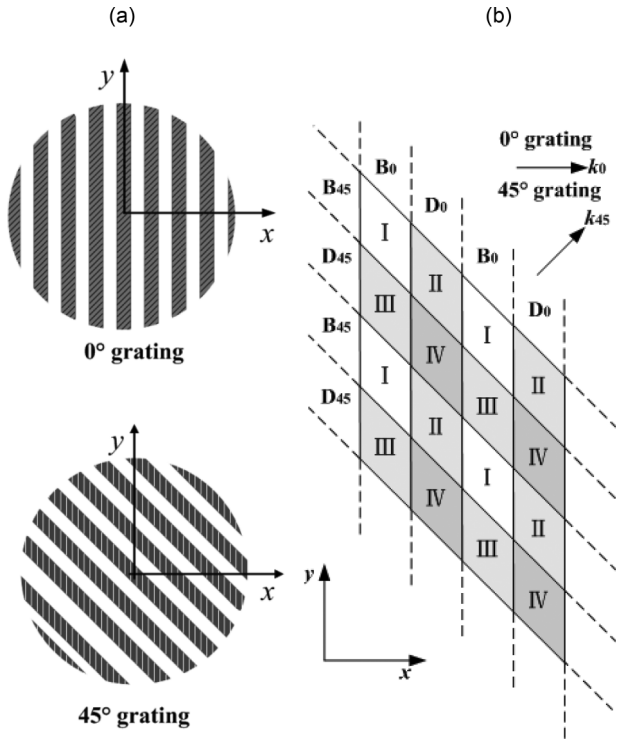

Figure 1. (a) Schematic representation of the multiplexed gratings for each corresponding exposure. Figure (b) Schematic overlapped regions for the 0° and 45° gratings. B_0 and D_0 are the corresponding bright and dark regions of the 0° grating. B_{45} and D_{45} are the corresponding bright and dark regions of the 45° grating. I, II, III, and IV are the overlapped regions of B_0 and B_{45}, D_0 and B_{45}, B_0 and D_{45}, D_0 and D_{45}, respectively.

illustrated in Figure 1(b). The time evolutions in the overlapped regions are illustrated for the period of $t = 40.0$~60.0 s, because most of the diffusion and polymerisation reactions take place during the second exposure time. In Figure 2(a), prior to the second exposure, because some of the free monomers are consumed in the first exposure, ϕ_M in II and IV are higher than those in I and III. At the beginning of the second exposure, i.e., $t = 40.0$~43.0 s, free monomers in II and IV have sufficient time and less difficulty to diffuse into I and III to equalise concentration gradient as the polymerisation process is not intense enough to block the travel of monomers. As a result, ϕ_M in I and III increases whereas ϕ_M in II and IV decreases. For the period of $t = 43.0$~60.0 s, the second exposure continues to take place, ϕ_M in I, II, III and IV decrease together since the free monomers continue to diffuse and to be polymerised. Furthermore, when $t = 52.0$~60.0 s, ϕ_M in III and IV are getting equal, so are ϕ_M in I and II. In Figure 2(b), ϕ_P in I, II, III and IV increase monotonically for the period of $t = 40.0$~60.0 s, and ϕ_P in I and II rises much faster than those of III and IV,

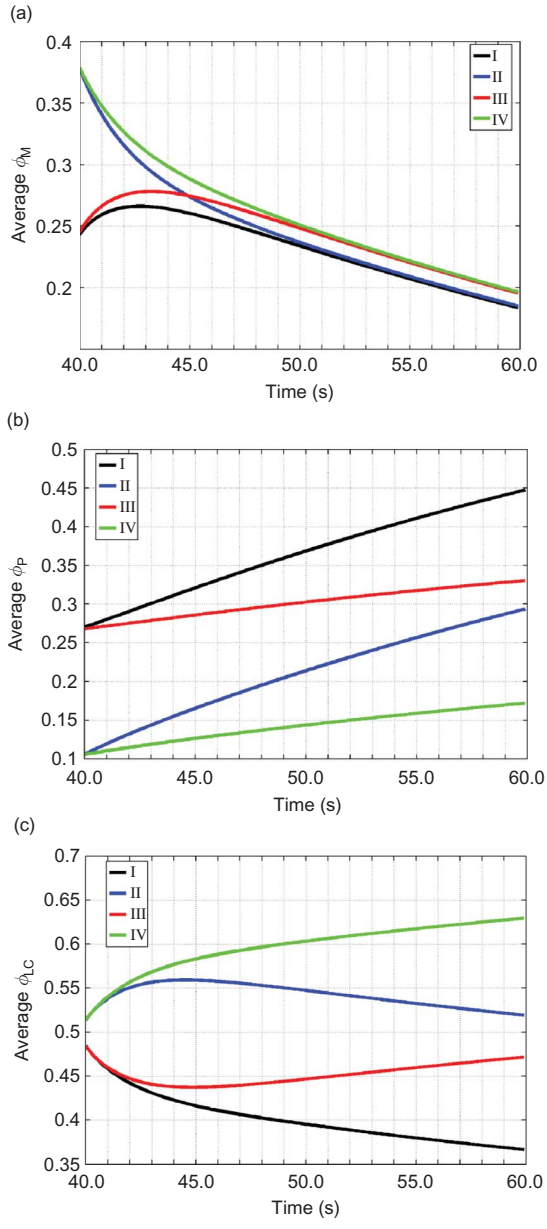

Figure 2. (colour online) Time evolution of the volume fraction for (a) free monomer, (b) polymer, and (c) LC in the overlapped regions of the 0° and 45° grating, when the exposure intensity I_0 = 2.5 mW cm^{-2}.

because more free monomers can be polymerised in the bright regions (I & II) of the 45° grating than in the dark regions (III & IV). In Figure 2(c), for the early period of t = 40.0~44.5 s, ϕ_{LC} in I and III first decrease because ϕ_M and ϕ_P increase. Meanwhile, ϕ_{LC} in II and IV increase as the free monomers in II and IV will diffuse to I and III as above mentioned, which makes the room for LC molecules to aggregate into II and IV. For t = 44.5~60.0, ϕ_{LC} in I and II keep decreasing because more and more free monomers will be polymerised in these regions forcing LC molecules to aggregate into III and IV, thereby causing continuous increase of ϕ_{LC} in these dark regions. More interestingly, we should notice that rates of change for I and IV and for II and III are equal in value but opposite in sign. This would infer an important conclusion that the diffusions of LCs are from I to IV always and from III to II at the beginning and then from II to III later on.

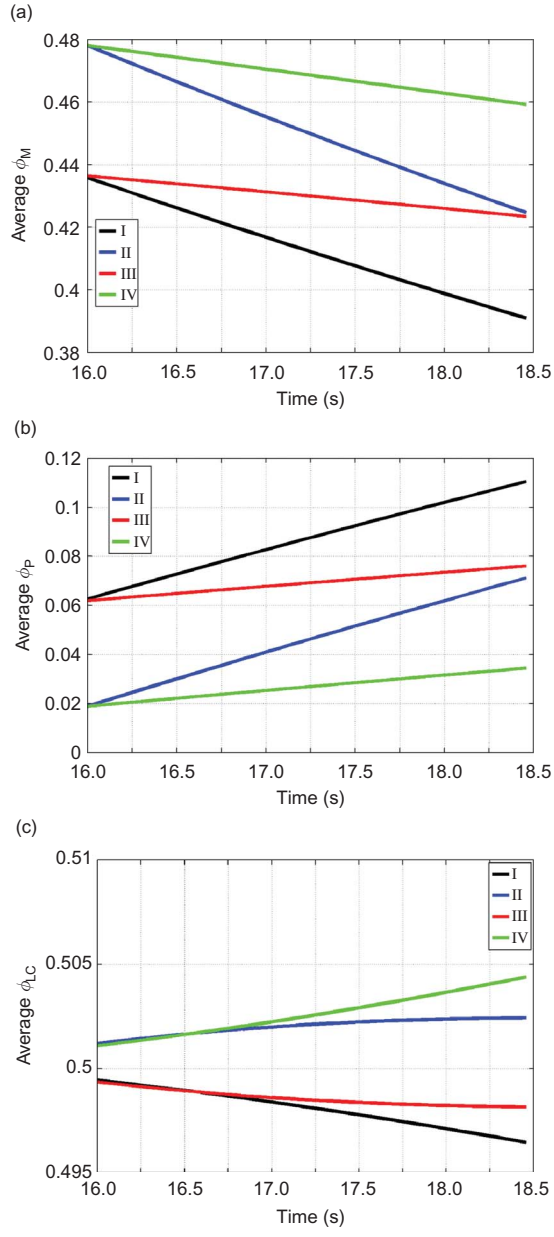

Figure 3. (colour online) Time evolution of the volume fraction for (a) free monomer, (b) polymer, and (c) LC in the overlapped regions of the 0° and 45° grating, when the exposure intensity I_0 = 19.6 mW cm^{-2}.

3.2 *Diffusion dynamics under the high intensity*

Figure 3 depicts the time evolution of the volume fraction of each material component within the overlapped regions of 0° and 45° gratings during the second exposure under I_0 = 19.6 mW cm^{-2}. The overlapped regions are referred as I, II, III, and IV as illustrated in Figure 1(b). The time evolutions in the overlapped regions are illustrated for the period of t = 16.0~18.5 s, because most of the diffusion and polymerisation reactions take place during the second exposure time. In Figure 3(a), before the second exposure, because some of the free monomers are consumed in the first exposure, ϕ_M in II and IV are higher than those in I and III, which resembles the case of I_0 = 2.5 mW cm^{-2}. The high exposure irradiance can cause relatively rapid polymerisation, and only a few free monomers in the dark regions can get sufficient time to diffuse into the bright regions of the 0° grating, before the polymerisation occurs. For the period of t = 16.0~18.5 s, ϕ_M in I, II, III and IV monotonously decreases. ϕ_M in the bright regions of the 45° grating (I and II) decrease much faster than that of dark regions (III and IV). In Figure 3(b), ϕ_P in I, II, III and IV increase monotonously. ϕ_P in the bright regions in the 45° grating (I and II) increase much faster than that of dark regions (III and IV). In Figure 3(c), for the period of t = 16.0~18.5 s, ϕ_{LC} in I decreases because some of the free monomers are polymerised and the average ϕ_P then increases. ϕ_{LC} in II increases slowly because a few free monomers can diffuse into I to be polymerised, meanwhile, the LC molecules aggregate into II. Only a few free monomers can diffuse into III to be polymerised and the LC molecules aggregate into II and IV, thus ϕ_{LC} in III decreases slowly. ϕ_{LC} in IV increases faster than II because some of the free monomers diffuse into the bright regions of 45° grating (I and II) to be polymerised and LC molecules aggregate into region IV.

3.3 *Time evolutions of ARI and RIM*

The time evolution of ARI and RIM for the 0° grating under I_0 = 2.5 mW cm^{-2} during the second exposure is shown in Figure 4(a). Prior to the second exposure, the ARI in the bright regions (I&II) is higher than that in the dark regions (III&IV). At the beginning of the exposure, a large number of the free monomers in the dark regions of the 0° grating can diffuse into the bright regions before the polymerisation reaction occurs. Meanwhile, the LC molecules can aggregate into the dark regions of the 0° grating from the bright regions, as shown in Figure 2(c). As a result, the decrease of ARI in the bright regions (dotted curve) along with the increase of ARI in the dark regions (dashed curve) of the 0° grating, will result in the decrease of RIM (solid curve) for the period of t = 40.0~41.2 s. The ARI of dark regions will then catches up with that of the bright regions, at which RIM equals zero, (t = 41.2 s). Subsequently, from t > 41.2 s, the ARI in the dark regions will exceed that in the bright regions, and the RIM continues to grow, even getting over the initial value at the beginning of the exposure after t = 46.2 s. By way of analogy, the above process can be described as a bounce, as RIM sharply drops to zero and then rises monotonically.

The time evolution of ARI and RIM for the 0° grating under I_0 = 19.6 mW cm^{-2} is shown in Figure 4(b). Before the second exposure takes place, the ARI in the bright regions is higher than that in the dark regions, which resembles the cases I_0 = 2.5 mW cm^{-2}. However, when the second exposure continues to take place, the free monomers in II and IV are difficult to diffuse into I and III to equalise the free monomer gradient concentration before the polymerisation reaction occurs, because the high-exposure irradiance can cause relatively rapid polymerisation process. Thus, most of free monomers are locked within the bright and dark regions to be polymerised later on, and only a few LC molecules can aggregate into II and IV. Therefore, the increase of ARI in the bright region (dotted curve) along with the increase of ARI in the dark region (dashed curve) of the 0° grating, results in the decrease of RIM (solid curve) for the period of t = 16.0~18.5 s. There are more free monomers being polymerised in the dark regions than in the bright regions. Since the ARI in the dark regions increases faster than that in the bright regions, the RIM drops monotonically in the absence of bounce.

As shown in Figure 4(b), during the first exposure, RIM decreases monotonically because high-exposure irradiance can cause rapid polymerisation kinetics. Furthermore, free monomers are difficult to diffuse from the dark regions into the bright regions of the 0° grating during the second exposure, and the possible explanations are given as the following reasons. (1) A relatively high-viscosity is caused due to the high-exposure intensity. During the conversion from monomers to polymers, the time varying viscosity effects due to densification and crosslinking, which can hinder the LC and free monomer molecules movement, will become more pronounced.[16,36] (2) High-intensity exposure can also cause a rapid depletion of dark regions. The high-exposure intensity not only causes a more rapid consumption of the free monomers, resulting in steep free monomer concentration gradients in bright regions, but also increases

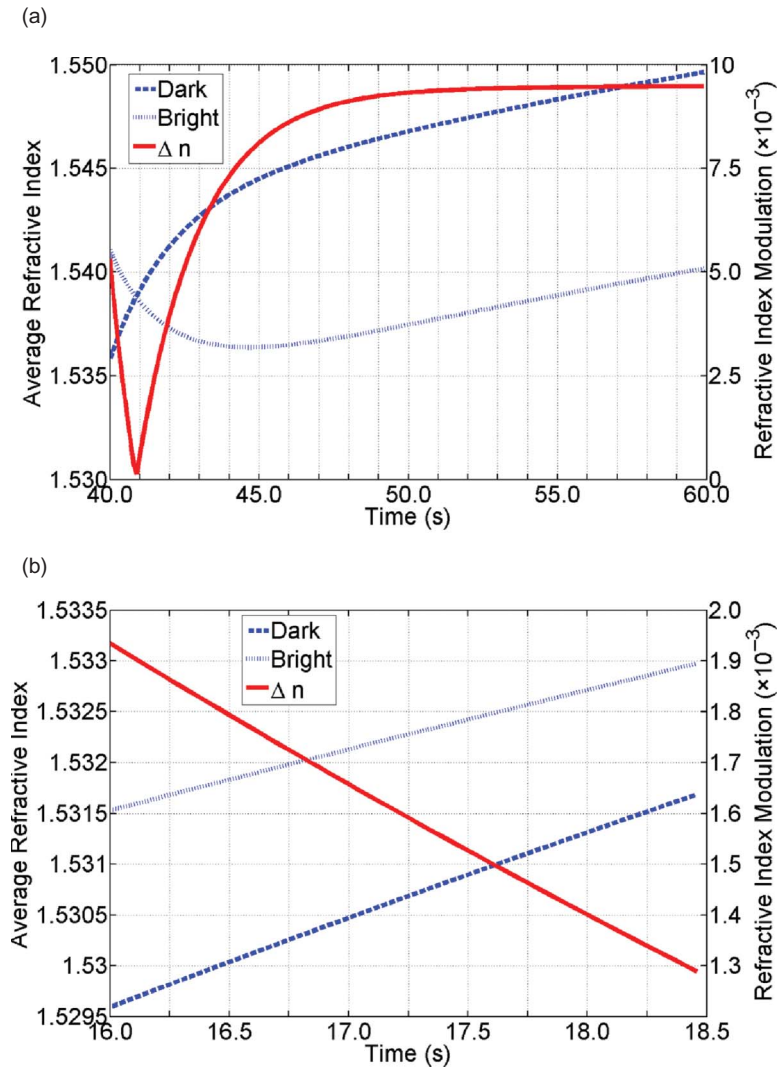

Figure 4. (colour online) Time evolution of the ARI in the bright regions (dotted curve) and in the dark regions (dashed curve) and RIM (solid curve) during the second exposure for the 0° grating. (a) Exposure intensity I_0 = 2.5 mW cm^{-2}, (b) Exposure intensity I_0 = 19.6 mW cm^{-2}.

the consumption of the free monomers on both borders of the dark regions.[10,30,36] Therefore, the available amount of the free monomers for diffusion is reduced under the high-exposure intensity during the second exposure.

4. Experimental results

To validate the time evolution of RIM based 2D model under the high and low intensities, 0°, 45°, and 90° grating are stored on the PDLC cell base on peristrophic multiplexing technique. In our experiments, the optical setup is schematically depicted in Figure 5. Both the reference beam and signal beam are sourced from a neodymium-doped yttrium aluminium garnet (Nd:YAG) laser (λ = 532 nm) with exposure intensities of I_0 = 2.5 mW cm^{-2} and 19.6 mW cm^{-2}, respectively, and the diameter of the exposure region is D = 3.0 mm. A He–Ne laser beam (λ = 632.8 nm), with an intensity of 0.1 mW cm^{-2} and D = 2.0 mm, is used to probe the writing region. These beams are both set to p-polarisation. During the experiments, each component of the PDLC mixture is listed as in Table 1, with mass fraction being specified. The cell is formed by attaching two glass substrates, with the thickness controlled by a Mylar spacer of 40.0 μm. The uniform mixture then is filled into the cell via the capillary action. In this experiment, peristrophic multiplexing is carried out by the rotation of the PDLC cell about the surface normal, instead of rotating the reference and signal beams. The holographic gratings are recorded under each

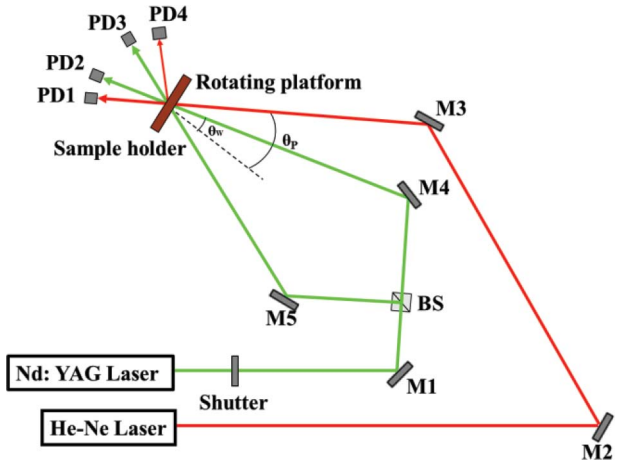

Figure 5. (colour online) Experimental setup for holographic storage, M1–M5: mirrors, BS: beam splitter, θ_w: incident angle for the recording holograms, θ_p: probe angle, PD1-PD4: photodiode detectors.

Table 1. Parameters used in the experiments.

Component	Mass fraction
TMPTA (Aldrich)	35.4 wt%
N-vinylpyrrollidone (Aldrich)	13.0 wt%
N-phenylglycine (Aldrich)	1.0 wt%
Rose Bengal (Aldrich)	0.6 wt%
LC (5CB, HCCH)	51.0 wt%

exposure at an incident angle of 15.0° corresponding to a grating period Λ = 1.03 μm. Then it is probed using the He–Ne laser at the Bragg angle of 15.7° through the photodiode detector PD4, and the transmitted beam is monitored by photodiode detector PD1. The PDLC cell was heated to 40–45°C, which is above the nematic-isotropic transition point of the 5CB. This is in order to prevent the appearance of a nematic phase during the curing process.[41] During the grating fabrication, the temporal variations of the transmitted recording beams are monitored through photodiode detectors PD2 and PD3. The diffraction efficiency of the Bragg grating is defined as the radio between the intensity of the diffracted light and the sum of diffracted and transmitted light.

The overall exposure time for I_0 = 2.5 mW cm^{-2}, and 19.6 mW cm^{-2} is t_{sum} = 40.0 s, and 16.0 s, respectively. The exposure times are denoted as t_1, t_2, and t_3 for the first, second and third exposure under each exposure intensity, respectively. The post-curing time is therefore $t_{sum} - t_i$, where i = 1, 2, 3. When I_0 = 2.5 mW cm^{-2}, the exposure time is $t_1 = t_2 = t_3$ = 20.0 s, When I_0 = 19.6 mW cm^{-2}, t_1 = 2.55 s, t_2 = 2.2 s, and t_3 = 2.0 s.

In further details, as shown in Figure 6(a), for low-exposure intensity (I_0 = 2.5 mW cm^{-2}), the diffraction efficiency for the 0° grating rises slowly and monotonically for the first holographic grating. The reason is that the applied low-exposure irradiance can cause slow polymerisation kinetics.[30] Then, at the beginning of the second exposure, the diffraction efficiency sharply drops to zero, and increases afterwards, i.e., the bounce of diffraction efficiency appears when t = 41.2 s, as shown in Figure 6(a). The diffraction efficiency for the 0° grating then further increases by more than 5% compared to the initial value of the 0° grating during the second exposure, i.e., around t = 60.0 s, $\bar{\eta}$ = 76%, and furthermore, we observed that around t = 100.0 s, $\bar{\eta}$ = 77%. During the third exposure in Figure 2(a), the diffraction efficiency for the 45° grating increases by 2%.

On the contrary, as shown in Figure 6(b), under the relatively high-exposure intensity condition (I_0 = 19.6 mW cm^{-2}), it is obvious that for the first exposure the diffraction efficiency rises much faster than that in the cases of I_0 = 2.5 mW cm^{-2}, due to the reason that high-exposure irradiance can cause relatively rapid polymerisation.[30] The first holographic grating is developed immediately during the first exposure. During the second exposure, the diffraction efficiency of the 0° grating starts to decrease from t = 16.0 to 18.2 s. The diffraction efficiency of the 0° grating then further decreases from t = 32.0 to 34.0 s during the third exposure. This tendency is opposite to the cases of I_0 = 2.5 mW cm^{-2}. With I_0 = 19.6 mW cm^{-2}, the equal-strength holograms are successfully recorded in the PDLC cell. To realise equal-strength holograms, sufficiently high-exposure intensity is required.

When the exposure intensity increases from 2.5 to 19.6 mW cm^{-2}, the polymerisation rate increases due to the highly increased photon absorption, hence the radicalisation. In details, the higher exposure intensity can cause a more rapid conversion from monomers to polymers. However, this behaviour also simultaneously increases the likelihood of termination processes, which can cause much more shortened polymer chains to be formed.[35] Furthermore, when at the low-exposure intensity for peristrophic multiplexed gratings, it is relatively easier for the free monomers to diffuse into the bright regions seeking further polymerisation, because the available regions for monomer diffusion due to concentration gradient are abundant.

Moreover, as can be observed that the simulation results agree well with the experimental data in Figures 6(a)–(b), and there is no significant variation for the value of D_0 extracted for the different exposure intensities, as given in Table 2. The average diffusion coefficient is estimated to be $D_0 = 7.95 \times 10^{-11}$ cm^2 s^{-1}. The main reason for the smaller value of the diffusion

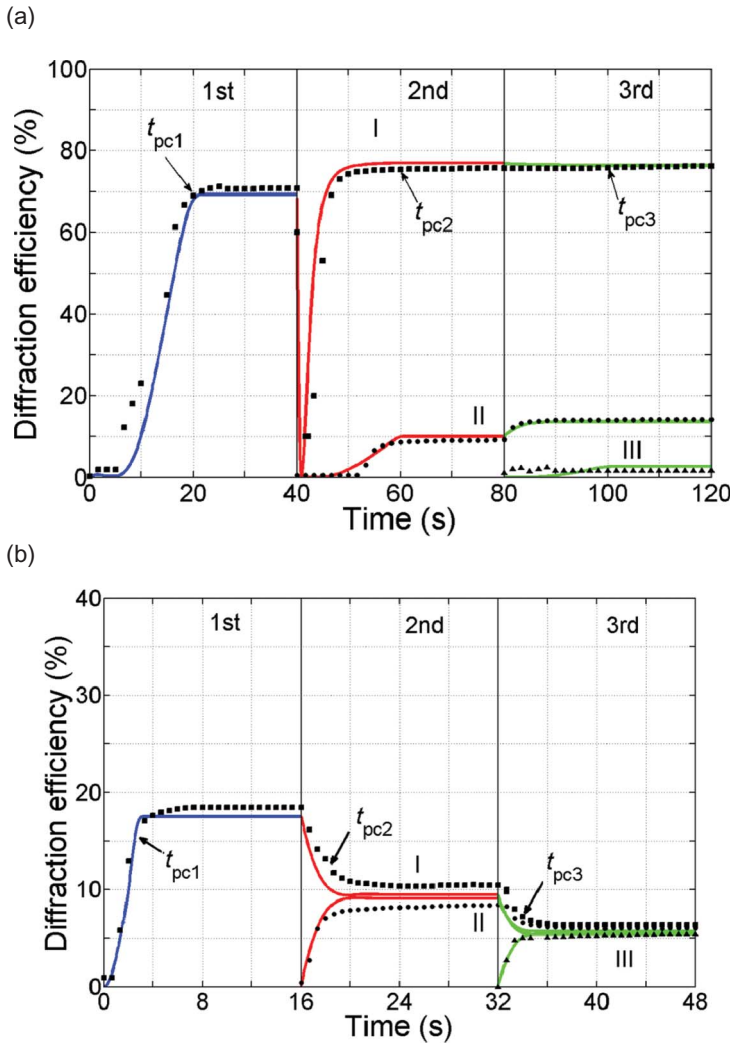

Figure 6. (colour online) Experimentally monitored diffraction efficiency with respect to exposure time for peristrophic multiplexed PDLC cell under three exposure intensities I_0: (a) I_0 = 2.5 mW cm^{-2}, (b) I_0 = 19.6 mW cm^{-2}, where black squares, circles and triangles denote the experimental results for the 0°, 45° and 90° grating, respectively. The solid curves denote simulation results for the 0°, 45° and 90° grating, respectively. 1st, 2nd and 3rd denote the first, second and third exposure, respectively. I, II, and III denote the 0°, 45° and 90° grating, respectively. t_{pc1}, t_{pc2} and t_{pc3} denote the start time of postcuring for the first, second and third exposure, respectively.

Table 2. Parameters values extracted from fittings to the growth curve record at different exposure intensity.

I_0 (mW cm^{-2})	κ cmmW$^{-\frac{1}{2}}$s^{-1}	D_0 ($\times 10^{-11}$cm^{2}s^{-1})	$\sqrt{\sigma}$ (nm)
2.5	0.010	7.89	90.9
19.6	0.012	8.01	82.3

coefficient obtained than the one presented in Ref.[8] is that the nonlocal effect has been taken into account. It is important to note that the relative consistency of the values obtained nonlocal response parameter. As has been observed, this PDLC material suffers significantly for nonlocal effect. The mean value presented in Table 2 for the nonlocal response parameter is determined to be $\sqrt{\sigma}$ = 86.6 nm for Λ = 1.03 μm. In the case of I_0 = 2.5 mW cm^{-2}, the erasing coefficient r_{11} = 0 is during the first exposure. r_{21} = 0.3 and r_{22} = 0.28 are the erasing coefficients for the 0° and 45° gratings during the second exposure, respectively. r_{31} = 0.01, r_{32} = 0.11, and r_{33} = 0.21 are the erasing coefficients for the 0°, 45° and 90° gratings during the third exposure, respectively. In the case of I_0 = 19.6 mW cm^{-2}, r_{11} = 0 is the erasing coefficient during the first exposure. r_{21} = 0.03 and r_{22} = 0.002 are the erasing coefficients for the 0° and 45°gratings during the second exposure, respectively. r_{11} = 0.01, r_{32} = 0.02, and r_{33} = 0.005 are the erasing coefficients for the 0°, 45° and 90° gratings during the third exposure, respectively.

5. Elimination of bounce

In the practical application of multiplexing, DE bounces are undesirable for recording the equal-strength holograms. To eliminate such an effect, the exposure intensities should be optimised. The total exposure time as well as the occurrence time of the bounce is presented against different intensities as in Figure 7. The exposure time is adjusted to ensure equal dosage (50.0 mJ cm^{-2}) to be delivered into the PDLC film under the different intensities for the first exposure. As shown in Figure 7(a), the curves denote the DEs for the 0° grating during the second exposure under the different intensities, and the exposure time t_2 = 4.0 s. Under I_0 = 2.0, 8.0, 15.0 mW cm^{-2}, and the bounces appear in the short period of time. However, under I_0 = 20.0 and 30.0 mW cm^{-2}, the bounce disappears. As depicted in Figure 7(b), the solid curve with circles denotes the exposure times for the 0° grating during the second exposure under the intensities from 1.0 to 40.0 mW cm^{-2}. The solid curve with squares denotes the occurrences of bounce for the 0° grating during the second exposure under the intensities from 1.0 to 18.0 mW cm^{-2}. It is found that when the exposure intensity increases up to I_0 = 18.0 mW cm^{-2}, the bounce starts to disappear. This verifies the results presented in Figure 6(b), where DEs of the 0° grating continually decrease during the second and third exposures. From this result, it is

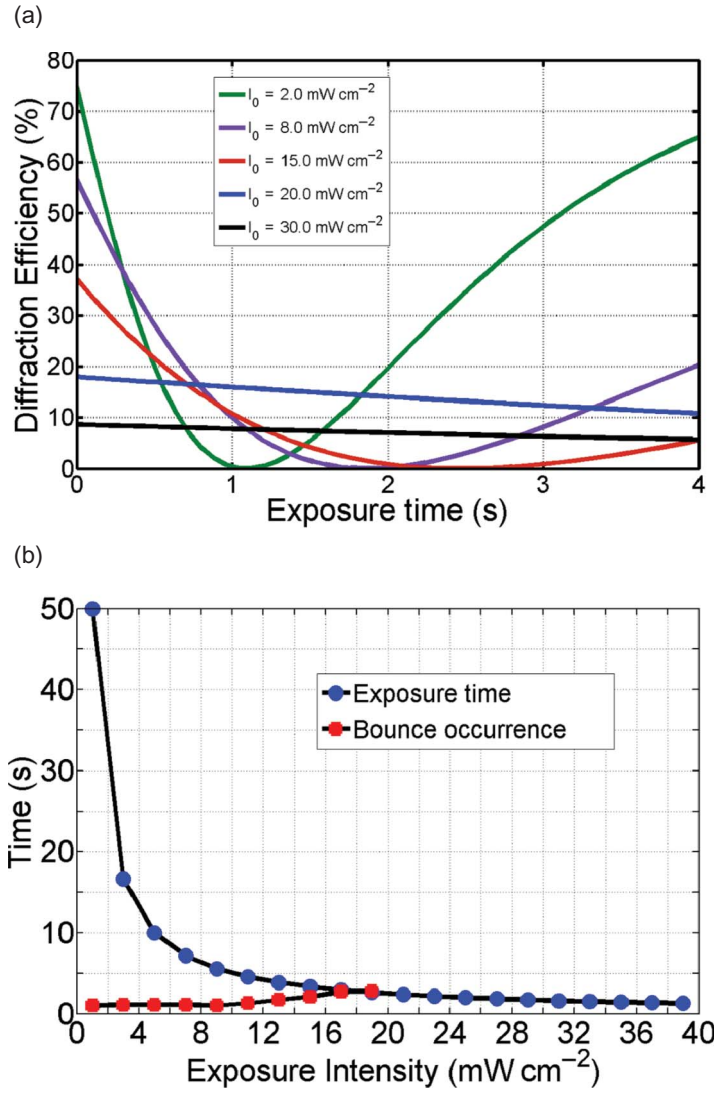

Figure 7. (colour online) (a) DEs for the 0° grating during the second exposure, and the exposure time t_2 = 4.0 s. when I_0 = 2.0, 8.0, 15.0, 20.0 and 30.0 mW cm^{-2} (green, orange, purple, blue and black curve, respectively), Figure (b). The exposure times (solid curve with circles) and the bounce occurrence (solid curve with squares) for the exposure intensities from 1.0 to 40.0 mW cm^{-2} during the second exposure for the 0° grating.

suggested that the exposure intensities for recording equal-strength hologram should exceed I_0 = 18.0 mW cm^{-2} to the PDLC material in our experiment. As discussed above, in order to realise the equal-strength holograms, the relative high-exposure intensities and relatively short exposure times are required in order to deliver sufficient energy for initiating appropriate polymerisation, instead of the relative low-exposure intensities and relatively long exposure times for each hologram to be recorded.

6. Conclusion

In this article, 2D nonlocal diffusion equations that describe multiplexed holographic grating formations in TMPTA-based PDLC cells are numerically solved using FDTD method. The proposed model explains the bounce of DE for multiple peristrophic multiplexed grating recording under the relatively low-exposure intensities. The occurrence of bounce is undesirable for recording equal-strength holograms, because the DE gaps between first and second gratings continuously enlarges. On the contrary, the DE of the first grating decreases monotonically under the high-exposure intensity, by which, the equal-strength holograms are recorded. A good agreement exists between the theoretically predicted and the experimentally measured DEs of the peristrophic multiplexed holographic gratings. This work is useful in realising equal-strength holograms for holographic storage.

Funding

This work was sponsored by 973 Program [grant number 2013CB328804]; NSFC [grant number 61307028], NSFC [grant number 61205183], [grant number 2013ZJ_0206]; Science and Technology Commission of Shanghai Municipality [grant number 11JC1405300], [grant number 13ZR1420000]; Fundamental Research Funds for the Central Universities [grant number XDJK 2011C047], and in part by Minhang Talent Program.

References

[1] Sutherland RL, Tondiglia VP, Natarajan LV, Bunning TJ. Evolution of anisotropic reflection gratings formed in holographic polymer-dispersed liquid crystal. Appl Phys Lett. 2001;79:1420–1422.
[2] Gao H, Pu H, Gao B, Yin D, Liu J, Gan F. Electrically switchable multiple volume hologram recording in polymer-dispersed liquid crystal films. Appl Phys Lett. 2009;95:201105.
[3] Liu Y, Sun X, Liu J, Dai H, Xu K. A polarization insensitive 2 × 2 optical switch fabricated by liquid crystal-polymer composite. Appl Phys Lett. 2005;86:041115.
[4] Caputo R, Sio LD, Veltri A, Umeton C, Sukhov AV. Development of a new kind of switchable holographic grating made of liquid-crystal films separated by slices of polymeric material. Opt Lett. 2004;29:1261–1263.
[5] Wu ST. Birefringence dispersions of liquid crystal. Phys Rev A. 1986;33:1270–1274.
[6] Bowley CC, Kossyrev PA, Crawford GP, Faris S. Variable-wavelength switchable Bragg gratings formed in polymer-dispersed liquid crystal. Appl Phys Lett. 2001;79:9–11.
[7] Caputo VR, Umeton C, Sukhov AV. Model for the photoinduced formation of diffraction gratings in liquid-crystalline composite materials. Appl Phys Lett. 2004;84:3492–3494.
[8] Pu H, Yin D, Gao B, Gao H, Dai H, Liu J. Dynamic characterizations of high diffraction efficiency in volume Bragg grating formed by holographic photopolymerization. J Appl Phys. 2009;106:083111.
[9] Rhee US, Caulfield HJ, Shamir J, Vikram CS, Mirsalehi MM. Characteristics of the DuPont photopolymer for angularly multiplexed page-oriented holographic memories. Opt Eng. 1993;32:1839–1847.
[10] Zhao G, Mouroulis P. Diffusion model of hologram formation in dry photopolymer materials. J Mod Opt. 1994;41:1929–1939.
[11] Wu SD, Glytsis EN. Characteristics of DuPont photopolymers for slanted holographic grating formations. J Opt Soc Am B. 2004;21:1722–1731.
[12] Wu SD, Glytsis EN. Holographic grating formation in photopolymers: analysis and experimental results based on a nonlocal diffusion model and rigorous coupled-wave analysis. J Opt Soc Am B. 2003;20:1177–1188.
[13] Sheridan JT, Lawrence JR. Nonlocal-response diffusion model of holographic recording in photopolymer. J Opt Soc Am A. 2000;17:1108–1114.
[14] Lawrence JR, O'Neill FT, Sheridan JT. Photopolymer holographic recording material parameter estimation using a nonlocal diffusion based model. J Appl Phys. 2001;90:3142–3148.
[15] Gleeson MR, Sheridan JT. Nonlocal photopolymerization kinetics including multiple termination mechanisms and dark reactions. Part I. Modeling. J Opt Soc Am B. 2009;26:1736–1745.
[16] Gleeson MR, Liu S, McLeod RR, Sheridan JT. Nonlocal photopolymerization kinetics including multiple termination mechanisms and dark reactions. Part II. Experimental validation. J Opt Soc Am B. 2009;26:1746–1754.
[17] Gleeson MR, Liu S, Guo J, Sheridan JT. Non-local photo-polymerization kinetics including multiple termination mechanisms and dark reactions: part III. Primary radical generation and inhibition. J Opt Soc Am B. 2010;27:1804–1812.
[18] Boots HMJ, Kloosterboer JG, Serbutoviez C, Touwslager FJ. Polymerization-induced phase separation. 1. Conversion-phase diagrams. Macromolecules. 1996;29:7683–7689.
[19] Serbutoviez C, Kloosterboer JG, Boots HMJ, Touwslager FJ. Polymerization-induced phase separation. 2. Morphology of polymer-dispersed liquid crystal thin films. Macromolecules. 1996;29:7690–7698.

[20] Serbutoviez C, Kloosterboer JG, Boots HMJ, Paulissen FAMA, Touwslager FJ. Polymerization-induced phase separation III. Morphologies and contrast ratios of polymer dispersed liquid crystals. Liq Cryst. 1997;22:145–156.
[21] Sutherland RL, Tondiglia VP, Natarajan LV, Bunning TJ. Phenomenological model of anisotropic volume hologram formation in liquid-crystal-photopolymer mixtures. J Appl Phys. 2004;96:951–965.
[22] Sutherland RL. Polarization and switching properties of holographic polymer-dispersed liquid-crystal gratings. I. Theoretical model. J Opt Soc Am B. 2002;19: 2995–3003.
[23] Sutherland RL, Tondiglia VP, Natarajan LV. Evolution of anisotropic reflection gratings formed in holographic polymer-dispersed liquid crystals. Appl Phys Lett. 2001;79:1420.
[24] Kyu T, Nwabunma D, Chiu HW. Theoretical simulation of holographic polymer-dispersed liquid-crystal films via pattern photopolymerization-induced phase separation. Phys Rev E. 2001;63:061802.
[25] Kyu T, Chiu HW. Morphology development during polymerization-induced phase separation in a polymer dispersed liquid crystal. Polymer. 2001;42:9173–9185.
[26] Kyu T, Meng S, Duran H, Nanjundiah K, Yandek GR. Holographic polymer-dispersed liquid crystals and polymeric photonic crystals formed by holographic photolithography. Macromol Res. 2006;14:155–165.
[27] Duran H, Meng S, Kim N, Hu J, Kyu T, Natarajan LV, Tondiglia VP, Bunning TJ. Kinetics of photopolymerization-induced phase separation and morphology development in mixtures of a nematic liquid crystal and multifunctional acrylate. Polymer. 2008;49:534–545.
[28] Yandek GR, Meng S, Sigalova GM, Kyu T. Three-dimensional switchable polymer photonic crystals via various optical wave interference techniques. Liq Cryst. 2006;33:775–788.
[29] Sutherland RL, Tondiglia VP, Natarajan LV, Bunning TJ, Adams WW. Electrically switchable volume gratings in polymer dispersed liquid crystals. Appl Phys Lett. 1994;64:1074–1076.
[30] Qi J, Li L, Sarkar MD, Crawford GP. Nonlocal photopolymerization effect in the formation of reflective holographic polymer-dispersed liquid crystals. J Appl Phys. 2004;96:2443–2450.
[31] Ren H, Wu ST. Inhomogeneous nanoscale polymer-dispersed liquid crystal with gradient refractive index. Appl Phys Lett. 2002;81:3537–3539.
[32] Bowley CC, Crawford GP. Diffusion kinetics of formation of holographic polymer-dispersed liquid crystal display materials. Appl Phys Lett. 2000;76:2235–2237.
[33] Kogelnik H. Coupled wave theory for thick hologram gratings. Bell Syst Tech J. 1969;48:2909–2946.
[34] Holmes ME, Malcuit MS. Controlling the anisotropy of holographic polymer-dispersed liquid-crystal gratings. Phys Rev E. 2002;65:066603.
[35] Liu Y, Sun X, Dai H, Liu J, Xu K. Effect of surfactant on the electro-optical properties of holographic polymer dispersed liquid crystal Bragg gratings. Opt Mater. 2005;27:1451–1455.
[36] Liu S, Gleeson MR, Guo J, Sheridan JT. High intensity response of photopolymer materials for holographic grating formation. Macromolecules. 2010;43: 9462–9472.
[37] Fernandez-Pousa CR, Carretero L, Fimia A. Dynamical behaviour of the optical properties of photopolymers and the Lorentz-Lorenz formula. J Mod Opt. 2000;47:1419–1433.
[38] Liu S, Gleeson MR, Guo J, Sheridan JT, Tolstik E, Matusevich V, Kowarschik R. Modeling the photochemical kinetics induced by holographic exposures in PQ/PMMA photopolymer material. J Opt Soc Am B. 2011;28:2833–2843.
[39] Lu YQ, Du F, Wu ST. Polarization switch using thick holographic polymer-dispersed liquid crystal grating. J Appl Phys. 2004;95:810–815.
[40] Aubrecht I, Miler M, Koudela I. Recording of holographic diffraction gratings in photopolymers: theoretical modelling and real-time monitoring of grating growth. J Mod Opt. 1998;45:1465–1477.
[41] Caputo R, Sio LD, Veltri A, Umeton C. Development of a new kind of switchable holographic grating made of liquid-crystal films separated by slices of polymeric material. Opt Lett. 2004;29:1261–1263.